An FFT-based Method for Attenuation Correction in Fluorescence Confocal Microscopy

J.B.T.M. Roerdink and M. Bakker
CWI
P.O. Box 4079, 1009 AB Amsterdam, The Netherlands

A problem in three-dimensional imaging by a confocal scanning laser microscope (CSLM) in the (epi)fluorescence mode is the darkening of the deeper layers due to absorption and scattering of both the excitation and the fluorescence light. In this paper we propose a new method to correct for these effects. Our approach, valid for weak attenuation, consists in multiplying the measured fluorescent intensity by a correction factor involving a convolution integral of the measured signal, which can be computed efficiently by the Fast Fourier Transform. We give analytical and numerical estimates as to the degree of attenuation under which our method is valid, and apply the method to various test images. We also show a restoration of a real CSLM image. Finally the method is compared with a recent iterative method with regard to numerical accuracy and computational efficiency.

AMS 1991 Mathematics Subject Classification: 68U10, 78A99.

Keywords: Fluorescence confocal microscopy, attenuation correction, convolution method, Fast Fourier Transform, 3D image processing.

Note: Postscript version obtainable at http://www.cs.rug.nl/~roe/. Final version appeared in: J. Microscopy 169, 1993, pp. 3-14.

1. Introduction

Three-dimensional (3D) images acquired with a confocal scanning laser microscope (CSLM) in the (epi)fluorescence mode [2,7] suffer from the darkening of the deeper layers in the object due to scattering and absorption of excitation and fluorescence light. A way has been devised to correct for this effect by a layer stripping method, where one iteratively corrects the first, second etc. layer, see Visser et al. [6]. They give a description of the problem in discrete space and discuss an implementation of the resulting algorithm. The process is more fully described below (see Section 6). A problem with this method is that it is very computer-intensive, because at the n-th layer one has to do a computation involving all the previous $n-1$ layers, for $n = 1, 2, ..., N_z$, where N_z is the number of vertical layers (i.e. the layers are orthogonal to the optical axis, which

is taken to coincide with the z-direction). This causes the computation time to scale as N_z^4. For an image of 16 layers, where each layer has a spatial resolution of 256 by 256 pixels, restoration by this layer stripping method may take as much as 10 hours on a RISC workstation. A modified algorithm where voxels (volume elements) in higher layers are 'condensed' by a kind of averaging procedure [6], still has complexity $\vee(N_z^2)$ and requires around one hour on the same workstation.

In this paper we develop a different solution to the attenuation problem. Following the model description of Visser et al., we reformulate the attenuation problem in continuous space. Next, assuming that the attenuation is weak, we construct by analytic methods a correction to the standard restoration, which takes the form of a multiplicative factor involving a 3D convolution of the measured signal. As is well known, such convolutions can be efficiently computed by the use of Fast Fourier Transform (FFT) methods. In this way, the complexity of computation is reduced to $\vee(N_z \log N_z)$. Taking the same example and hardware as mentioned above, the computation time using our method is reduced to around 8 minutes. To further reduce the computation time one may resort to the use of dedicated hardware for fast convolution.

To establish the limit of validity of our method we performed several analytical and numerical estimates. The accuracy of the results depends on the depth of the layer considered: deeper layers are less accurately reconstructed than higher layers. Test results indicate that an intensity drop of 25% going from the top layer to the bottom layer can be corrected for to within 5% or less. When the attenuation becomes as high as 50% the method becomes less accurate, but is still able to reduce this attenuation to about 25%.

The organization of this paper is as follows. In Section 2 we sketch the imaging process of the CSLM and formulate this in mathematical terms as a nonlinear integral transform of the object function. In Section 3 we perform a perturbation expansion based upon the assumption of weak attenuation, yielding a correction factor in the form of a convolution integral. The discretization of the correction integral is discussed and some details on its numerical computation by the FFT are given. The accuracy of the method is studied in Section 4 by applying it to a test function which varies only in the z-direction so that its integral transform can be accurately calculated and the results can be compared to the known values. Analytical estimates for the general case are given in an Appendix. In Section 5 we apply our method to several artificially constructed test images as well as a real image from a confocal microscope, and show the resulting restored images. We also make an assessment of the restoration accuracy and present some timing results concerning the computational efficiency of the algorithm, including a comparison with the layer stripping method mentioned above.

2. Mathematical formulation of the imaging process

We start our discussion by a short description of the imaging process of a CSLM operating in the fluorescence mode. For more details, see e.g. [2,7]. The experimental set-up is shown in Figure 1. A laserbeam is focussed upon a pinhole, expanded again and, through a system of lenses, focussed upon a point in the object. The width of the incoming bundle is characterized by a semi-aperture angle ω, which may be as large as 60° in practice. The radiation absorbed at the point in focus is reemitted as fluorescent radiation.

This is achieved by labeling the object to be imaged with fluorochromes (particles of fluorescent material). This fluorescent radiation is emitted uniformly in all directions. Part of it therefore travels back the same route as the incoming radiation until it reaches a so-called dichroic mirror, which deflects this radiation towards the detector where the total radiation in the bundle is measured. The object is discretized into a number N_z of layers along the optical axis, a distance δ_z apart. The total depth of the sample is denoted by d_z. Also, each layer is discretized into a rectangular grid of N_x by N_y points, with spacings δ_x and δ_y in the x- and

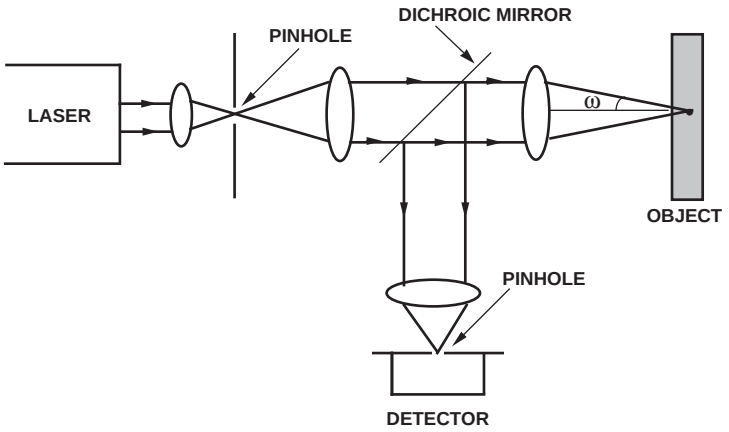

Figure 1. *Sketch of the confocal microscope in fluorescence mode.*

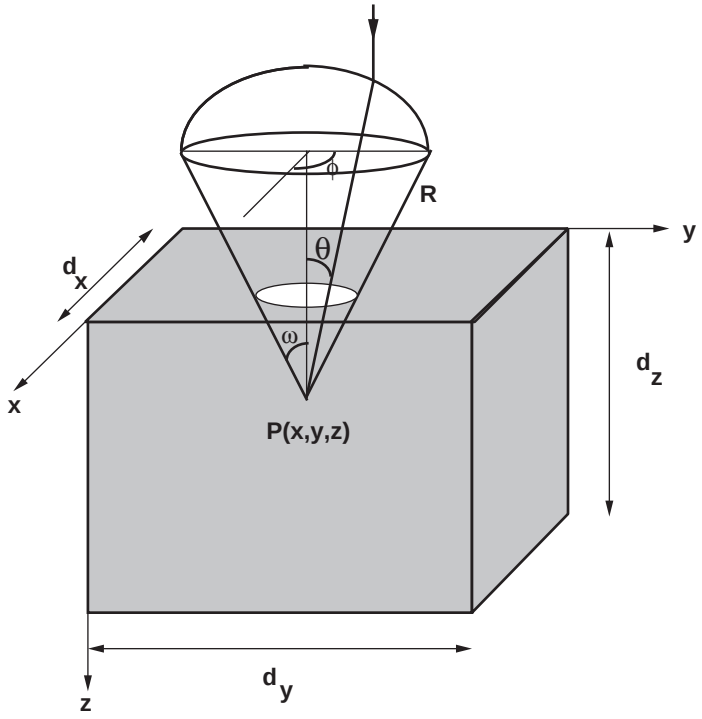

Figure 2. *Geometry of light cone with apex at a point $P(x, y, z)$ in the object.*
R: radius of spherical bundle; ω: semi-aperture angle; (θ, ϕ): polar angles of light ray; d_z: depth of the sample. The optical axis coincides with the z-axis.

y-direction, respectively. By moving the scan table of the CSLM each objectpoint of the 3D grid so formed is brought into focus and the corresponding fluorescent intensity (energy per unit of time) measured.

We now proceed to formalize the above description in a mathematical way. Our treatment closely follows [6] to which we refer for details on the assumptions underlying the model and

their physical justification.

The incoming bundle, with intensity per unit area denoted by I, converges to the object point as a spherical bundle of radius R. The reader is referred to Figure 2, where the direction of the incoming bundle (the positive z-direction) is drawn downward. Hence the object extends over the range $0 \leq z \leq d_z$ in the vertical direction. The total intensity I_0 of the bundle therefore satisfies the relation

$$I_0 = \int_0^{\omega} d\theta \ \sin\theta \int_0^{2\pi} d\phi \ IR^2 \cos\theta = \pi I R^2 \sin^2\omega. \tag{2.1}$$

Here θ is the angle of a light ray with the z-axis, and the $\cos\theta$ factor stems from the fact that a uniform incoming bundle converges to a spherical bundle. As is seen from Figure 2, the rays converging to the object point are contained in a circular cone ('light cone') with angle ω.

Attach a fixed Cartesian coordinate system to the object, and let the point in focus be denoted by $\mathbf{r} := (x, y, z)$. Also, introduce a polar coordinate system moving along with the objective. The total attenuation of a ray along the line segment with polar angles θ and ϕ (with respect to the optical axis) and arriving at $\mathbf{r}$ is determined by the line integral,

$$l(\theta, \phi; x, y, z) = \int_0^z \frac{dz'}{\cos\theta} \ a\left(x + (z - z')\tan\theta\cos\phi, \ y + (z - z')\tan\theta\sin\phi, \ z'\right), \tag{2.2}$$

where, for any point $\mathbf{r}'$ of the object, $a(\mathbf{r}')$ is the attenuation coefficient at that point. The total excitation intensity $I_e(\mathbf{r})$ arriving at the point $\mathbf{r}$ can be written as a superposition of contributions along rays ending in $\mathbf{r}$:

$$I_e(\mathbf{r}) = \int_0^{\omega} d\theta \ \sin\theta \int_0^{2\pi} d\phi \ IR^2 \cos\theta \ \exp\left[-l(\theta, \phi; x, y, z)\right]. \tag{2.3}$$

It is convenient to define a forward attenuation coefficient $\gamma_f(\mathbf{r})$ by

$$\gamma_f(\mathbf{r}) := \frac{I_e(\mathbf{r})}{I_0} = \frac{1}{\pi \sin^2\omega} \int_0^{\omega} d\theta \ \int_0^{2\pi} d\phi \ \sin\theta\cos\theta \exp\left[-l(\theta, \phi; x, y, z)\right]. \tag{2.4}$$

The definition is chosen in such a way that γ_f reduces to unity when the attenuation is zero everywhere.

The excitation light is transferred into fluorescent light with an efficiency $\alpha\rho(\mathbf{r})$, where $\rho(\mathbf{r})$ depends on the density of fluorochromes at the point $\mathbf{r}$ and α is a proportionality constant. The intensity of emitted fluorescent light is therefore

$$I_f(\mathbf{r}) = \alpha\rho(\mathbf{r}) I_e(\mathbf{r}). \tag{2.5}$$

The fluorescent light is isotropically emitted and the part which travels back the same way as the incoming radiation is detected. Let this detected intensity corresponding to the point $\mathbf{r}$ in focus be denoted by $F(\mathbf{r})$. Then, assuming that the attenuation coefficient of the excitation light equals that of the fluorescence light, we get

$$F(\mathbf{r}) = \int_0^{\omega} d\theta \int_0^{2\pi} d\phi \ \sin\theta \ \frac{1}{4\pi} I_f(\mathbf{r}) \exp\left[-l(\theta, \phi; x, y, z)\right]. \tag{2.6}$$

Note that the extra factor '$\cos\theta$' in Eq.(2.3) is absent here because of the assumption of isotropic emission.

Define a backward attenuation factor $\gamma_b(\mathbf{r})$ by

$$\gamma_b(\mathbf{r}) := \frac{2F(\mathbf{r})}{(1-\cos\omega)I_f(\mathbf{r})} = \frac{1}{2\pi(1-\cos\omega)}\int_0^{\omega} d\theta \int_0^{2\pi} d\phi \ \sin\theta \ \exp\bigl[-l(\theta,\phi;x,y,z)\bigr], \quad (2.7)$$

which again equals unity if there is no attenuation. Combining the results so far we have

$$F(\mathbf{r}) = \frac{1}{2}\gamma_f(\mathbf{r})\gamma_b(\mathbf{r})\alpha(1-\cos\omega)I_0\rho(\mathbf{r}). \quad (2.8)$$

Define the normalized signal f by

$$f(\mathbf{r}) := \frac{2F(\mathbf{r})}{\alpha I_0(1-\cos\omega)} = \gamma_f(\mathbf{r})\gamma_b(\mathbf{r})\rho(\mathbf{r}). \quad (2.9)$$

This equation shows that $\rho(\mathbf{r})$ is the fluorescent density which would be measured if the attenuation was completely absent. Our eventual aim is to perform an attenuation correction of the measured signal, or, in other words, to reconstruct the density ρ from f. The attenuation factors in (2.9) still contain the unknown function $a(\mathbf{r})$. To proceed, we assume that $a(\mathbf{r})$ is functionally dependent upon the density $\rho(\mathbf{r})$:

$$a(\mathbf{r}) = g(\rho(\mathbf{r})). \quad (2.10)$$

In some cases, such as DNA labeled with fluorochromes, the attenuation is (approximately) proportional to the fluorescent density:

$$g(\rho(\mathbf{r})) \propto \rho(\mathbf{r}), \quad (2.11)$$

while in other cases, such as geological sandstone samples, a relation of the form

$$g(\rho(\mathbf{r})) = \begin{cases} a_1 & \rho(\mathbf{r}) \le h \\ \\ a_2 & \rho(\mathbf{r}) > h \end{cases} \quad (2.12)$$

is assumed [6]. Here the extinction at the stone points (small fluorescent density) is larger than at the points in the fluorescent liquid (high fluorescent density), i.e. $a_1 > a_2$.

We observe that instead of reconstructing the density $\rho(\mathbf{r})$ one may also reconstruct the attenuation function $a(\mathbf{r})$ as done by Visser et al. [6]. Eq. (2.10) shows that, if $\rho(\mathbf{r})$ has been obtained, one only has to compute $g(\rho(\mathbf{r}))$ in each point $\mathbf{r}$ to obtain the desired result. For the case of linear attenuation the two densities are essentially identical.

Inserting the attenuation factors in (2.9) we get

$$\begin{aligned} f(\mathbf{r}) = \rho(\mathbf{r}) &\times \frac{1}{\pi\sin^2\omega}\int_0^{\omega} d\theta \int_0^{2\pi} d\phi \ \sin\theta \ \cos\theta \ \exp\left[-\int_0^z \frac{dz'}{\cos\theta}\, g\left(\rho(\hat{r})\right)\right] \\ &\times \frac{1}{2\pi(1-\cos\omega)}\int_0^{\omega} d\theta \int_0^{2\pi} d\phi \ \sin\theta \ \exp\left[-\int_0^z \frac{dz'}{\cos\theta}\, g\left(\rho(\hat{r})\right)\right], \end{aligned} \quad (2.13)$$

where $\hat{r}$ is the vector

$$\hat{r}(\mathbf{r};\theta,\phi,z') = (x + (z-z')\tan\theta\cos\phi, \ y + (z-z')\tan\theta\sin\phi, \ z'). \quad (2.14)$$

This formula expresses the measured signal f as a nonlinear integral transform of the unknown density ρ. Since there is little hope to find an explicit analytical solution of this equation, we follow an approach which is based on the assumption of weak attenuation, meaning that the exponential factors in this equation are 'small' in some sense.

To make precise what is meant by 'small' in this case, it is essential to introduce a quatitative measure for the degree of attenuation. It is clear that the amount of attenuation will depend on the first place on the values of the function g in Eq. (2.10). This can be quantified by introducing the following 'norm' $\|g\|$ of the function g, which measures the maximum value of g over the 3D region V occupied by the sample:

$$\|g\| = max_{\mathbf{r}\in V}\ g(\rho(\mathbf{r}))\,. \tag{2.15}$$

Secondly, the total attenuation of a light ray—for a given maximum value of g—depends on the total depth d_z of the sample. This implies that a measure for the degree of attenuation of the signal when traversing the $complete$ sample is provided by the dimensionless parameter

$$\epsilon := \|g\|\, d_z\,. \tag{2.16}$$

Now introduce a dimensionless depth variable $\tilde{z} = z/d_z$ running between 0 and 1, and define a normalized attenuation function $\tilde{g}$ by

$$\tilde{g}(\mathbf{r}) := g(\rho(\mathbf{r}))/\,\|g\|\,. \tag{2.17}$$

Then the two exponential factors in Eq. (2.20) can be rewritten as

$$\exp\left[-\,\|g\|\, d_z \int_0^{\tilde{z}} \frac{d\tilde{z}'}{\cos\theta}\ \tilde{g}\left(\rho(\tilde{\hat{r}})\right)\right], \tag{2.18}$$

where $\tilde{\hat{r}}$ is defined by

$$\tilde{\hat{r}}(\tilde{\mathbf{r}};\theta,\phi,\tilde{z}') = (x + (\tilde{z}-\tilde{z}')\tan\theta\cos\phi,\ y + (\tilde{z}-\tilde{z}')\tan\theta\sin\phi,\ \tilde{z}'). \tag{2.19}$$

This shows that as a result of the renormalization a prefactor of the form $\epsilon = \|g\|\, d_z$ emerges. To simplify the notation, we drop all the tildes again but assume for the rest of this paper that the renormalizations of the attenuation function g and the depth variable z have already taken place, so that the final result for the measured signal coincides with Eq. (2.13) apart from the addition of a factor ϵ in the exponents:

$$\begin{aligned} f(\mathbf{r}) = \rho(\mathbf{r}) \times \frac{1}{\pi\sin^2\omega}\int_0^{\omega} d\theta \int_0^{2\pi} d\phi\ \sin\theta\ \cos\theta\ \exp\left[-\epsilon\int_0^{z}\frac{dz'}{\cos\theta}\ g\left(\rho(\hat{r})\right)\right] \\ \times \frac{1}{2\pi(1-\cos\omega)}\int_0^{\omega} d\theta \int_0^{2\pi} d\phi\ \sin\theta\ \exp\left[-\epsilon\int_0^{z}\frac{dz'}{\cos\theta}\ g\left(\rho(\hat{r})\right)\right]. \end{aligned} \tag{2.20}$$

It should be noted that if the physical scale of the sample is modified, without changing the ratios between the dimensions in the x-, y- and z-directions, this is accounted for by a modified value of ϵ without changing the form of (2.20). The same holds for (additional) rescalings of f, g or ρ.

3. Approximate inversion of the integral transform

In this section we will find an approximate solution of the basic equation (2.20) by using the standard mathematical technique of perturbation expansion in a small parameter. The basic idea is simple: from Eq. (2.20) one sees that the solution $\rho(\mathbf{r})$ will be a function of—among others—the variable ϵ, so that one can write

$$\rho(\mathbf{r}) = \rho(\mathbf{r};\epsilon)\,, \tag{3.1}$$

to explicitly indicate this ϵ-dependence. If attenuation could be completely neglected then we would have $\epsilon = 0$ and hence $\rho(\mathbf{r}) = \rho(\mathbf{r};0) = f(\mathbf{r})$, that is the restored signal equals the measured signal. Now if the attenuation is nonzero but small, as determined by the magnitude of ϵ, then we can perform a Taylor expansion of $\rho(\mathbf{r};\epsilon)$ in the parameter ϵ, and retain only the lowest order terms, which requires that $\epsilon << 1$. When only the term which is linear in ϵ is retained we get an attenuation correction of the restored signal to first order in ϵ. This first order term in ϵ turns out to involve a convolution integral of the measured signal f which can be evaluated efficiently by FFT methods. Needless to say the application of this method in practice will only be justified if the attenuation, that is, the parameter ϵ, is indeed small. The question of how large an error is commited for a given value of ϵ will be taken up in Section 4.

Weak attenuation expansion

As a starting point we expand $\rho(\mathbf{r})$ in powers of ϵ,

$$\rho(\mathbf{r}) = \rho_0(\mathbf{r}) + \epsilon\rho_1(\mathbf{r}) + \epsilon^2\rho_2(\mathbf{r}) + ..., \tag{3.2}$$

substitute this in (2.20) and collect terms of like powers in ϵ. Putting ϵ equal to zero results in

$$f(\mathbf{r}) = \rho_0(\mathbf{r}). \tag{3.3}$$

Next we collect terms of first order in ϵ. This yields

$$0 = \rho_1(\mathbf{r}) - \rho_0(\mathbf{r}) \left[\int_0^\omega d\theta \int_0^{2\pi} d\phi \ \sin\theta \ \int_0^z \frac{dz'}{\cos\theta} \left(C_f \cos\theta + C_b\right) \ g\left(\rho_0(\hat{r}(\mathbf{r};\theta,\phi,z'))\right) \right], \tag{3.4}$$

where

$$C_f := \frac{1}{\pi \sin^2\omega}, \quad C_b := \frac{1}{2\pi(1-\cos\omega)}, \tag{3.5}$$

are the normalization constants referring to the forward and backward attenuation factors, respectively. Hence, to first order in ϵ we find the following approximation $\tilde{\rho}(\mathbf{r})$ for the density:

$$\tilde{\rho}(\mathbf{r}) = f(\mathbf{r}) \left\{1 + \epsilon \ c(\mathbf{r})\right\}, \tag{3.6}$$

where $c(\mathbf{r})$ is defined by

$$c(\mathbf{r}) = \int_0^{2\pi} d\phi \int_0^\omega d\theta \ \left(C_f \sin\theta + C_b \tan\theta\right) \int_0^z dz' \ g\left(f(\hat{r}(\mathbf{r};\theta,\phi,z'))\right). \tag{3.7}$$

Convolution form

Next we show that (3.7) can be written as a 3D convolution. Recalling that

$$\hat{r}(\mathbf{r};\theta,\phi,z') = (x + (z-z')\tan\theta\cos\phi, \ y + (z-z')\tan\theta\sin\phi, \ z'),$$

we perform a change of variables, $\{\theta,\phi\} \to \{x',y'\}$, where

$$\begin{aligned} x' &= x + (z-z')\tan\theta\cos\phi, \\ y' &= y + (z-z')\tan\theta\sin\phi. \end{aligned} \tag{3.8}$$

The Jacobian of this transformation is

$$J = \left| \begin{array}{cc} \frac{\partial x'}{\partial\theta} & \frac{\partial x'}{\partial\phi} \\ \frac{\partial y'}{\partial\theta} & \frac{\partial y'}{\partial\phi} \end{array} \right| = \left| \begin{array}{cc} (z-z')\frac{\cos\phi}{\cos^2\theta} & -(z-z')\tan\theta\sin\phi \\ (z-z')\frac{\sin\phi}{\cos^2\theta} & (z-z')\tan\theta\cos\phi \end{array} \right| = (z-z')^2\frac{\tan\theta}{\cos^2\theta}. \tag{3.9}$$

Hence we get, after interchanging the order of integration,

$$c(\mathbf{r}) = \int_0^z dz' \oint_{B(x,y;r)} dx'dy' \frac{\cos^2\theta}{(z-z')^2 \tan\theta} \left(C_f \sin\theta + C_b \tan\theta\right) g\left(f(x',y',z')\right), \quad (3.10)$$

where $B(x,y;r)$ denotes the disc with center (x,y) and radius r. Here r is given by

$$r = (z-z')\tan\omega, \quad (3.11)$$

and $\oint_{B(x,y;r} dx'\,dy'$ is a shorthand notation to indicate that the x',y'-integration is to be carried out over the disc $B(x,y;r)$. Performing another change of variables, $\mathbf{r}' = (x',y',z') \to \mathbf{r}'' = (x'',y'',z'')$, where

$$x'' = x - x' \quad y'' = y - y' \quad z'' = z - z',$$

and using that, for $\theta \le \omega \le \pi/2$,

$$\cos\theta = (1+\tan^2\theta)^{-1/2} = \left[\frac{z''^2}{x''^2+y''^2+z''^2}\right]^{1/2}, \quad (3.12)$$

we find

$$\begin{aligned} c(\mathbf{r}) &= \int_0^z dz'' \oint_{B(0,0;z''\tan\omega)} dx''\,dy'' \frac{1}{z''^2}\left(C_f\cos^3\theta + C_b\cos^2\theta\right) g\left(f(\mathbf{r}-\mathbf{r}'')\right) \\ &= \int_0^z dz' \oint_{B(0,0;z'\tan\omega)} dx'\,dy' \left(C_f \frac{z'}{(x'^2+y'^2+z')^{3/2}} + C_b \frac{1}{x'^2+y'^2+z'^2}\right) g\left(f(\mathbf{r}-\mathbf{r}')\right). \end{aligned} \quad (3.13)$$

Finally, making use of the fact that the density $\rho(x,y,z)$ is zero for $z<0$ or $z>d$, we can write (3.13) manifestly as a convolution integral:

$$c(\mathbf{r}) = \int_{-\infty}^{\infty}\int_{-\infty}^{\infty}\int_{-\infty}^{\infty} d\mathbf{r}'\ \kappa(\mathbf{r}')\ g\left(f(\mathbf{r}-\mathbf{r}')\right), \quad (3.14)$$

where $\kappa(\mathbf{r})$ is the space-invariant kernel given by

$$\kappa(x,y,z) = \begin{cases} C_f \frac{z}{(x^2+y^2+z^2)^{3/2}} + C_b \frac{1}{x^2+y^2+z^2}, & 0 \le z \le d_z,\ x^2+y^2 \le (z\tan\omega)^2 \\ 0 & \text{elsewhere} \end{cases} \quad (3.15)$$

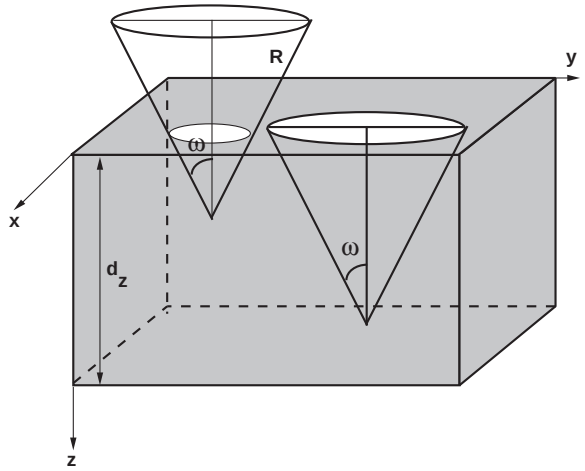

Figure 3. *The correction term $c(\mathbf{r})$ is obtained by putting the light cone at point $\mathbf{r}$ and performing the convolution of the signal function with the kernel (3.15), which has support inside this light cone of height d_z.*

This formula shows that the kernel $\kappa(\mathbf{r})$ has support in the circular light cone of height d_z. The value of the convolution at a point $\mathbf{r}$ is obtained by putting this cone with its apex at $\mathbf{r}$ and calculating the convolution of the kernel function inside the cone with the signal function $g\left(f(\mathbf{r})\right)$, see Figure 3.

The divergence of $\kappa(\mathbf{r})$ at $\mathbf{r} = \mathbf{0}$ is harmless since the support of the kernel also goes to zero there (apex of the cone). For example, one easily checks that the integral of $\kappa(\mathbf{r})$ over the cone is finite and equals $2d_z$.

Numerical computation

To evaluate the integral (3.14) numerically, we subdivide the region of interest into a grid of $N_x \times N_y \times N_z$ voxels, each voxel being a box of dimensions $\delta_x, \delta_y, \delta_z$ in the x-, y- and z-directions, respectively, and assume the signal function $f(\mathbf{r})$ to have a constant value in each voxel. Define the 3D arrays R, C, F and G by

$$\begin{aligned} R_{ijk} &:= \tilde{\rho}\left(i\delta_x, j\delta_y, k\delta_z\right), \\ C_{ijk} &:= c\left(i\delta_x, j\delta_y, k\delta_z\right), \\ F_{ijk} &:= f\left(i\delta_x, j\delta_y, k\delta_z\right), \\ G_{ijk} &:= g(F_{ijk}), \end{aligned} \tag{3.16}$$

for $i = 1, .., N_x; j = 1, .., N_y; k = 1, .., N_z$. Then the approximation (3.6) is replaced by

$$R_{ijk} = F_{ijk}(1 + \epsilon\ C_{ijk}), \tag{3.17}$$

and the integral (3.14) by the discrete convolution

$$C_{ijk} = \sum_{i'=-\frac{M_x}{2}+1}^{\frac{M_x}{2}} \sum_{j'=-\frac{M_y}{2}+1}^{\frac{M_y}{2}} \sum_{k'=1}^{M_z} K_{i'j'k'}\ G_{i-i',j-j',k-k'}, \tag{3.18}$$

where K is the discrete counterpart of the convolution kernel (3.15),

$$\begin{aligned} K_{ijk} &:= \int_{(i-\frac{1}{2})\delta_x}^{(i+\frac{1}{2})\delta_x} dx \int_{(j-\frac{1}{2})\delta_y}^{(j+\frac{1}{2})\delta_y} dy \int_{(k-1)\delta_z}^{k\delta_z} dz\ \kappa(x,y,z) \\ &\approx \delta_x\delta_y\delta_z\ \kappa\left(i\delta_x, j\delta_y, (k-1/2)\delta_z\right). \end{aligned} \tag{3.19}$$

Here M_x, M_y, M_z denote the support of the kernel in the three space directions in units of $\delta_x, \delta_y, \delta_z$, respectively. So $M_z = d_z/\delta_z = N_z$, where d_z is the depth of the sample, and similarly, $M_x = 2d_z \tan(\omega)/\delta_x, M_y = 2d_z \tan(\omega)/\delta_y$, where in all cases rounding off to integer values is understood. The different treatment of the x, y-summations versus the z-summation stems from the fact that the kernel is symmetric in the x, y-directions, while it extends only over non-negative values in the z-direction. To obtain sufficient accuracy of this discretization it is required that the grid is taken fine enough.

As is well known, one can evaluate the discrete convolution (3.18) efficiently by FFT methods. Care has to be taken to make sure that appropriate zero padding of the signal G and the kernel K is performed in order to avoid undesired wrap around effects, see e.g. [3], where the convolution kernel is called the 'response function' and the function to be convolved the 'signal function'. In our case, the convolution kernel extends over the complete depth of the sample, so that zero padding results in a doubling of the arrays in the vertical dimension, while in the x, y-directions the signal array C_{ijk} has to be extended by amounts $M_x/2, M_y/2$, respectively. The response function K_{ijk} is also extended by zeros to make the dimensions equal to those of the zero-padded signal array, where the i and j indices have to be renumbered in wrap around order to make them run over non-negative integers only [3].

The restoration procedure

The complete procedure of reconstructing the fluorescent density from measured data as developed above contains the following steps:

1. Read the data $F_{ijk}, i = 1, .., N_x, j = 1, .., N_y, k = 1, .., N_z$ from a file.
2. Compute the convolution C_{ijk} of the data $G_{ijk} = g(F_{ijk})$ with the kernel K_{ijk}.
3. Determine the appropriate value of the attenuation constant ϵ.
4. Compute the endresult according to the approximation (3.6).

Input parameters of the algorithm are the dimensions N_x, N_y, N_z of the data array, the scanning steps $\delta_x, \delta_y, \delta_z$, the semi-aperture angle ω and the attenuation constant ϵ. For the determination of the correct value of ϵ one may resort to a calibration experiment in which a homogeneous test sample is used [6]. In this paper we will consider test densities for which the value of ϵ is known.

4. Accuracy of the method

Our restoration method as outlined in the previous section contains two sources of inaccuracy: first the error involved in using the approximation (3.6), second the error caused by the discretization into voxels, necessary for applying the discrete convolution algorithm. In order to assess the importance of the first error source we consider a spatially constant test function ρ, for which the signal density (2.20) and the approximate inversion formula can be expressed in terms of a one-dimensional integral which can be evaluted to high numerical precision (no discrete convolution used). In particular we investigate the range of values of the attenuation parameter ϵ for which the approximation (3.6) gives a satisfactory representation of the exact result. Conclusions reached from this test function do not necessarily hold for more complicated density functions, but may give a first indication of the accuracy to be expected. Restorations of spatially varying density functions using the discrete convolution algorithm are considered in the next section.

To substantiate the outcome of this numerical experiment we present in an Appendix some analytical error estimates which enable us to make a more general assessment of the error caused by truncating the expansion (3.2).

Restoration of a test function

Consider a test function which has a constant value ρ_0 (depth $d_z = 1$),

$$\rho(x, y, z) = \rho_0, \quad 0 \leq z \leq 1. \tag{4.1}$$

For the functional dependence of $g(\rho)$ as a function of ρ we consider the following three cases, as typical representatives of the kind of behaviour which one may encounter in practice:

$$\begin{aligned} &\text{(i)} \quad g\,(\rho) = \rho \\ &\text{(ii)} \quad g\,(\rho) = e^{-\rho} \\ &\text{(iii)} \quad g\,(\rho) = \rho e^{-\rho}. \end{aligned} \tag{4.2}$$

The signal function f (which depends on the depth z only) corresponding to this density is (see Eq. (2.20))

$$f(z) = \rho_0 \gamma_f(z) \gamma_b(z), \tag{4.3}$$

where the corresponding forward and backward attenuation factors are given by

$$\gamma_f(z) = \frac{2\pi}{\pi \sin^2\omega} \int_0^\omega d\theta \ \sin\theta \cos\theta \exp\left(-\int_0^z \frac{dz'}{\cos\theta}\ \epsilon\ g(\rho_0)\right)$$
$$\gamma_b(z) = \frac{2\pi}{2\pi(1-\cos\omega)} \int_0^\omega d\theta \ \sin\theta \exp\left(-\int_0^z \frac{dz'}{\cos\theta}\ \epsilon\ g(\rho_0)\right). \tag{4.4}$$

Performing a change of variable, $x = \cos\theta$, we get

$$\gamma_f(z) = \frac{2}{\sin^2\omega} I_1(z), \quad \gamma_b(z) = \frac{1}{1-\cos\omega} I_0(z), \tag{4.5}$$

where

$$I_0(z) = \int_{\cos\omega}^1 dx\ e^{-\epsilon g(\rho_0) z/x},$$
$$I_1(z) = \int_{\cos\omega}^1 dx\ x e^{-\epsilon g(\rho_0) z/x} = \frac{1}{2}\left[e^{-\epsilon g(\rho_0) z} - \cos^2\omega\ e^{-\epsilon g(\rho_0) z/\cos\omega} - \epsilon g(\rho_0) z I_0(z)\right] \tag{4.6}$$

So all quantities can be expressed in terms of the 1D integral $I_0(z)$, the so-called 'exponential integral' [1], which can be evaluated from tables or computed numerically.

The approximate restoration, denoted by $\tilde{\rho}_\epsilon$ to indicate the ϵ-dependence, is given by

$$\tilde{\rho}_\epsilon(z) = \rho_0 \gamma_f(z) \gamma_b(z) \{1 + \epsilon\ c(z)\}, \tag{4.7}$$

where, using (3.7) and (4.3),

$$\epsilon\ c(z) = \epsilon \int_0^{2\pi} d\phi \int_0^\omega d\theta \left(\frac{\sin\theta}{\pi \sin^2\omega} + \frac{\tan\theta}{2\pi(1-\cos\omega)}\right) \int_0^z dz'\ g\left(\rho_0 \gamma_f(z') \gamma_b(z')\right)$$
$$= \beta \int_0^z dz'\ g\left(\rho_0 \gamma_f(z') \gamma_b(z')\right), \tag{4.8}$$

with β given by

$$\beta = \epsilon \left(\frac{2(1-\cos\omega)}{\sin^2\omega} - \frac{\log(\cos\omega)}{1-\cos\omega}\right). \tag{4.9}$$

One easily infers from the formulas above that the restoration $\tilde{\rho}_\epsilon(z)$ depends on ϵ and z through the combination ϵz only,

$$\tilde{\rho}_\epsilon(z) = \tilde{\rho}_1(\epsilon z). \tag{4.10}$$

In other words, a small value of ϵ may be counterbalanced by a large depth z, which is in agreement with the observation below that the restoration accuracy of our approximate method decreases with increasing depth. Also, it is sufficient to vary either ϵ or z, so we will express all results in terms of the 'effective' depth variable ϵz.

In Table 1 we present the results of the restorations for the three cases (4.2). We have chosen $\epsilon = 0.5, d_z = 1.0$, so that a substantial attenuation is obtained at the deepest level. In all cases we use $N_z = 10$ depth levels. We observe that indeed the accuracy decreases with increasing depth. The (maximum) value of ϵz permitted if a given accuracy is to be attained can be easily determined from Table 1 for the various cases.

		case (i)		case (ii)		case (iii)	
ϵz	$\rho(z)$	$f(z)$	$\tilde{\rho}_\epsilon(z)$	$f(z)$	$\tilde{\rho}_\epsilon(z)$	$f(z)$	$\tilde{\rho}_\epsilon(z)$
0.00	1.000	1.000	1.000	1.000	1.000	1.000	1.000
0.05	1.000	0.873	0.984	0.951	0.999	0.951	0.998
0.10	1.000	0.762	0.944	0.905	0.995	0.905	0.991
0.15	1.000	0.666	0.889	0.861	0.990	0.861	0.981
0.20	1.000	0.582	0.827	0.819	0.983	0.819	0.968
0.25	1.000	0.509	0.761	0.779	0.974	0.779	0.952
0.30	1.000	0.445	0.694	0.741	0.964	0.741	0.934
0.35	1.000	0.390	0.629	0.705	0.952	0.705	0.914
0.40	1.000	0.341	0.568	0.671	0.940	0.671	0.893
0.45	1.000	0.298	0.510	0.639	0.926	0.639	0.870

Table 1. *Originals $\rho(z)$, signal values $f(z)$ and restorations $\tilde{\rho}_\epsilon(z)$ as a function of ϵz.*
Case (i): $g(\rho) = \rho$; case (ii): $g(\rho) = \exp(-\rho)$; case (iii): $g(\rho) = \rho\exp(-\rho)$.

¿From these results we conclude that our method is able to yield a substantial attenuation correction, especially for those cases in which the attenuation function $g(\rho)$ decreases for large ρ. Also we observe that the restoration error increases roughly linearly with the product ϵz, in agreement with the error analysis in the Appendix.

The next question is how our method works in the case of spatially varying densities. This is the subject of the next section.

5. Restoration of 3D images

In this section the restoration of 3D images is studied. First we artificially construct some test images and compare the original with the restored images for several values of ϵ, so that an assessment of the accuracy can be made. Then we show also a restoration of a real CSLM image.

Restoration of test images

We consider test densities $\rho(\mathbf{r})$, which vary in the x- and y-directions, but not in the z-direction. To find the corresponding signal values $f(\mathbf{r})$ according to Eq. (2.20), multiple integrals have to be computed numerically for every voxel of the test image to be generated, which takes a lot of CPU-time for realistic image sizes. By taking test images which are z-independent, the z-integrals in (2.20) can be computed analytically, reducing the computation time to generate the test images. Moreover, restorations of the deeper layers can be simply compared to the first layer for assessing the restoration accuracy.

First we discuss the case of a sinusoidally varying test image, referred to as 'trig image' below,

$$\rho(\mathbf{r}) = \frac{1}{4}\cos(2\pi n_x x/d_x)\ \cos(2\pi n_y y/d_y)\,, \tag{5.1}$$

where d_x and d_y are the spatial dimensions of the sample in the x- and y-directions, and n_x, n_y are integers determining the spatial frequencies. The values used below are $n_x = n_y = 8$.

In order to mimick practical densities with discontinuities, we have taken a second test image, 'circle image' for short, consisting of a number of circles with different grey values, also constant in the z- direction.

First we look at the computational efficiency of our algorithm. In Table 2 we present under 'FFT method' the result of some timing experiments of the algorithm by varying, for various sizes $N_x = N_y$ of a single image plane, the number N_z of vertical layers. For the FFT method, vertical layer numbers *before* zero padding are given, so that the convolution is actually performed with an N_z-value which is twice as large (see Section 3). Displayed is the total CPU time (sum of system and user time), which includes time used for data I/O (reading/writing of 3D image data from/to file). Times are given in minutes (m) and seconds (s). Computations were performed on a SPARC workstation (35 Mhz, 26 MIPS). We observe that the computational time is roughly proportional to the number N_z of vertical layers, in agreement with the well known complexity $\vee(N_z \log N_z)$ of the FFT.

We also did the timing for the layer stripping method of Visser et al. [6], where, starting with the first layer for which $R_{ij1} = F_{ij1}$ by assumption, one successively corrects the second layer, the third layer, etc. by computing a discrete approximation to the attenuation factors γ_f and γ_b involving the previous layers. The θ, ϕ-space is discretized into a number, say N_θ values of θ ('rings') and N_ϕ values of ϕ ('segments'). This poses the problem of two discretizations, one in θ, ϕ space, and one in ordinry 'voxel-space', which have to be brought into correspondence (in [6] this is done by creating a look-up table which determines to which segment of which ring each Cartesian point (i, j, k) belongs). Naturally, this causes discretization errors which are non-uniform throughout the sample. Also, it is not obvious how to choose N_θ or N_ϕ, which are extra input parameters of the algorithm. In the FFT method, this problem does not occur, because there we only work with the voxel discretization. Moreover, the layer stripping method is very computer-intensive, because at the n-th layer one has to do a computation involving all the previous $n-1$ layers. Calculating back from a given voxel, the number of voxels inside the light cone which need to be considered at the n-th layer is proportional to n^3, causing the computation time to scale as N_z^4, where N_z is the number of vertical layers. This effect is especially severe when ω is large ('high aperture'), which is the case considered here. Therefore in [6] a condensation procedure was used in which, by an averaging procedure, one effectively takes in each of the previous layers a *constant* number of 'effective' voxels into account, so that the computation time scales as N_z^2. Timing results for this modified layer stripping algorithm ($N_\theta = 8, N_\phi = 8, \delta_z/\delta_x = 4$) have been included in Table 2. We emphasize that the numbers in the Table have a limited value, since they depend on machine type, computational load of the network during runtime, etc. However, inspection of the numbers does confirm the approximate linear versus quadratic increase in computation time for the FFT method and the layer stripping method, respectively.

N_x	N_z	FFT method	layer method
64	8	$14s$	$50s$
	16	$27s$	$3m27s$
	32	$55s$	$14m21s$
	64	$1m50s$	$60m17s$
128	8	$56s$	$3m15s$
	16	$1m59s$	$13m41s$
	32	$4m14s$	$62m48s$
	64	$9m26s$	$251m57s$
256	8	$4m14s$	$13m24s$
	16	$8m27s$	$56m15s$

Table 2. *Timing results (CPU time) of the FFT method and the layer stripping method, for various values of N_x $(= N_y)$ and N_z.*

Next we consider the restoration accuracy. For both types of test images types we have calculated the signal data F_{ijk} by numerically computing the integrals in Eq.(2.20) for a number of equidistant 3D positions. The discretizations used in these computations were much finer than the voxel discretization, so that we can regard them as 'exact' data. For the attenuation function we chose the form $g(\rho) = \rho$, which is the 'hardest' of the cases considered in Section 4. The dimensions of the images were chosen as follows: $d_x = d_y = 1.0, d_z = 0.1$, $N_x = N_y = 128$, $N_z = 8$, and the semi-aperture taken as $\omega = 1.04719$. The resulting data array was then used as input to the convolution algorithm as described in Section 3.

We show the results in Figures 4 and 5. The first row contains the attenuated test images $f(\mathbf{r})$, the second and third row the restorations $\tilde{\rho}(\mathbf{r})$ by the FFT method and layer stripping method, respectively. In each row, the first, fourth and seventh layer is displayed from left to right, out of a total of 8 depth layers. Recall that the original image $\rho(\mathbf{r})$ in each layer is identical to the first image in row 1. We observe a considerable enhancement of the restored images over the attenuated images. The common practice of simply rescaling the grey-values in each layer to the same maximum level (say 255) is avoided here, in order to achieve a correct assessment of the restoration quality of our algorithm. Apart from that, contrast enhancement is not obtained by such rescalings anyway.

Finally, to quantify the restoration quality we computed the relative root mean square error

$$\mathcal{E}(z) := \left(\frac{\sum_{x=1}^{N_x} \sum_{y=1}^{N_y} \{\rho(x,y,z) - \tilde{\rho}(x,y,z)\}^2}{\sum_{x=1}^{N_x} \sum_{y=1}^{N_y} \{\rho(x,y,z)\}^2} \right)^{\frac{1}{2}}, \tag{5.2}$$

between original and restored image at each plane $z = constant$, again comparing our method with the layer stripping method. We found that for spatially constant test images the layer stripping method is much more accurate than the FFT method, which is not surprising since for constant densities the condensation operation makes no difference, so that in effect the exact layer stripping algorithm is performed. The accuracy for the FFT method is about the same as found in Section 4, meaning that the voxel discretization used has sufficient resolution.

However, for spatially varying test densities the situation changes considerably, see Tables 3 and 4, where the restoration error is displayed for the trig image ($\epsilon = 0.5$) and the circle image ($\epsilon = 0.3$), respectively. For comparison we give in column 2 of the Tables the error *before* restoration, denoted by 'signal error' and computed according to (5.2) with $\tilde{\rho}$ replaced by f. The corresponding errors after restoration are denoted by 'FFT error' and 'layer error' for the FFT method and the layer stripping method, respectively.

ϵz	signal error	FFT error	layer error
0.0000	0.000	0.000	0.000
0.0625	0.116	0.016	0.009
0.1250	0.217	0.054	0.022
0.1875	0.305	0.112	0.058
0.2500	0.382	0.181	0.101
0.3125	0.450	0.254	0.161
0.3750	0.509	0.326	0.229
0.4375	0.560	0.393	0.301

Table 3. *Signal error and restoration error as a function of the effective depth ϵz for the trig image.*

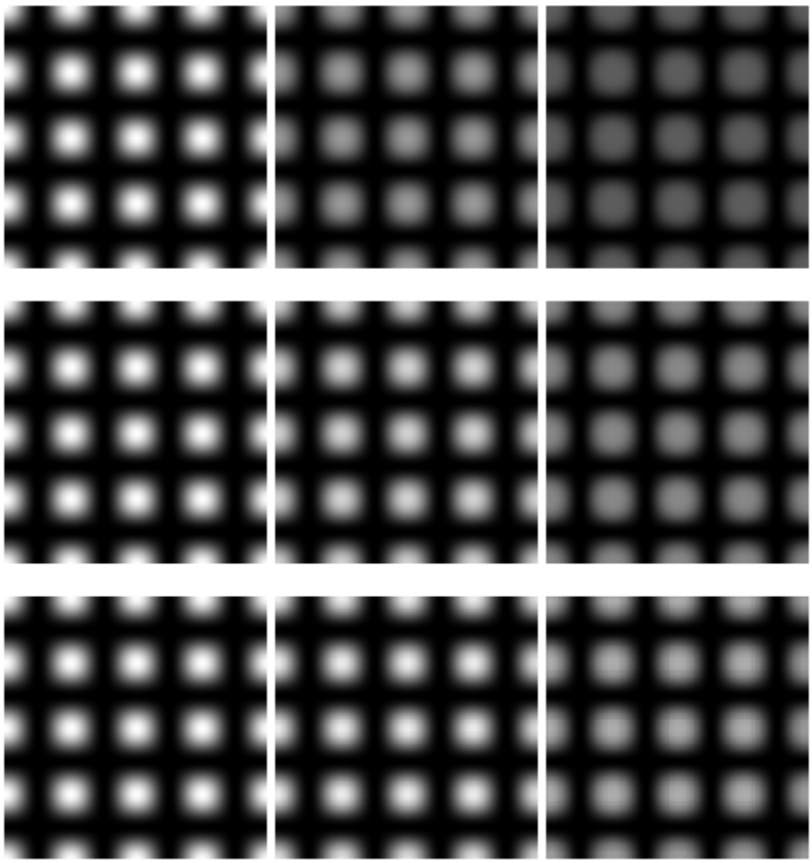

Figure 4. *Restoration of the trigonometric image.*
First row: the attenuated test images; second row: restoration by the FFT method; third row: restoration by the layer stripping method. In each row, the first, fourth and seventh layer is displayed from left to right. The original image in each layer is identical to the first image in row 1. Restoration errors are given in Table 3.

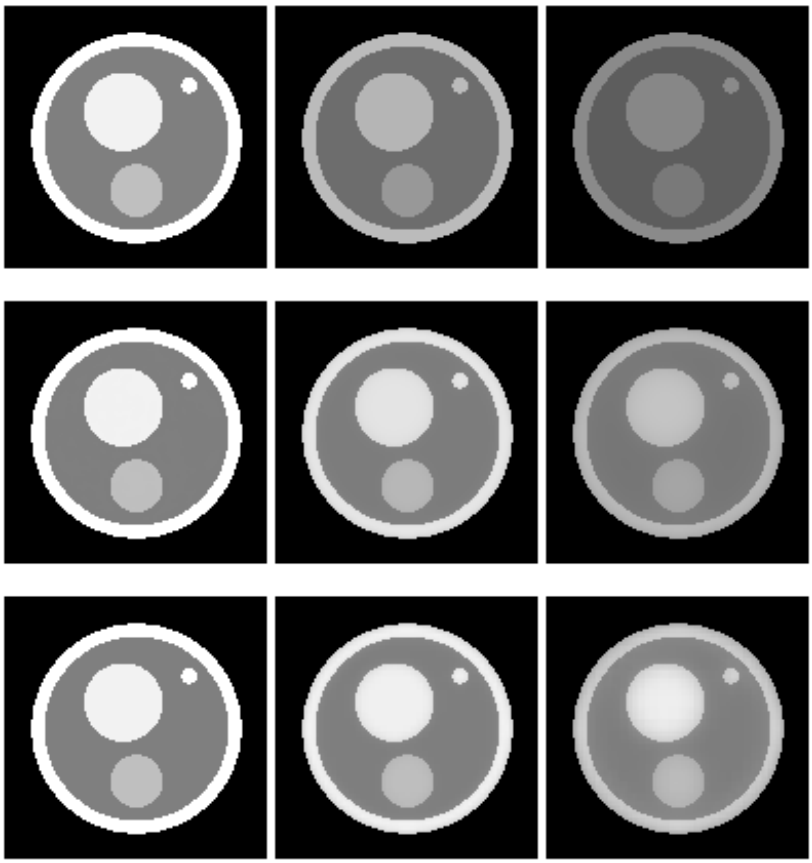

Figure 5. *Restoration of the circle image.*
First row: the attenuated test images; second row: restoration by the FFT method; third row: restoration by the layer stripping method. In each row, the first, fourth and seventh layer is displayed from left to right. The original image in each layer is identical to the first image in row 1. Restoration errors are given in Table 4.

ϵz	signal error	FFT error	layer error
0.000	0.000	0.000	0.000
0.025	0.086	0.017	0.016
0.050	0.162	0.044	0.034
0.075	0.233	0.084	0.062
0.100	0.297	0.130	0.094
0.125	0.355	0.176	0.127
0.150	0.408	0.226	0.165
0.175	0.454	0.271	0.200

Table 4. *Signal error and restoration error as a function of the effective depth ϵz for the circle image.*

We conclude that in the cases of the circle and trig images the layer stripping method remains more accurate than our method, but the quality becomes comparable at the deeper layers. Moreover, it has been observed in other contexts that layer stripping methods are noise sensitive: errors made in the firs layers will propagate to deeper layers [5]. In view of the great increase in computational efficiency of the FFT method we therefore conclude that the method developed here is a serious alternative for the layer stripping method.

Restoration of a real CSLM image

The method of this paper was applied to a CSLM image ($N_x = N_y = 256$, $N_z = 8$) of a geological sample consisting of sandstone cavities filled with a fluorescent oily substance, also considered in [6]. The result is shown in Figure 6. Clearly a substantial improvement is obtained, showing the practical usefulness of the method. We determined the value of ϵ in this case by trial and error: the value was chosen so as to give a visually satisfactory restoration. More work is needed to develop methods for the automatic determination of ϵ, preferably from the measured data itself.

6. Discussion

In this paper we describe a method for attenuation correction in Fluorescence Confocal Microscopy using Fast Fourier Transform methods. Our approach consists in multiplying the measured fluorescent intensity by a correction factor involving a convolution integral of the measured signal, which can be computed efficiently by an FFT-based algorithm. Our method is valid for weak attenuation. We give analytical and numerical estimates as to the degree of attenuation under which our method is valid. The accuracy of the results depends on the depth of the layer considered: deeper layers are less accurately reconstructed than higher layers. For the case of attenuation function $g(\rho)$ which vary linearly with ρ, test results indicate that an intensity drop of 25% going from the top layer to the bottom layer can be corrected for to within 5% or less. When the attenuation becomes as high as 50% the method becomes less accurate, but is still able to reduce this attenuation to about 25%. For attenuation functions which go to zero for large ρ, the restoration accuracy is considerably better. Application of the method on spatially varying test densities gives similar results.

We also compared the computational efficiency of our algorithm with the layer stripping method of [6]. In its original form this method has computational complexity $\vee(N_z^4)$, N_z being the number of vertical layers, and hence is unacceptably slow, taking many hours on a RISC workstation for a $256 \times 256 \times 16$ image [6]. The layer stripping method 'with

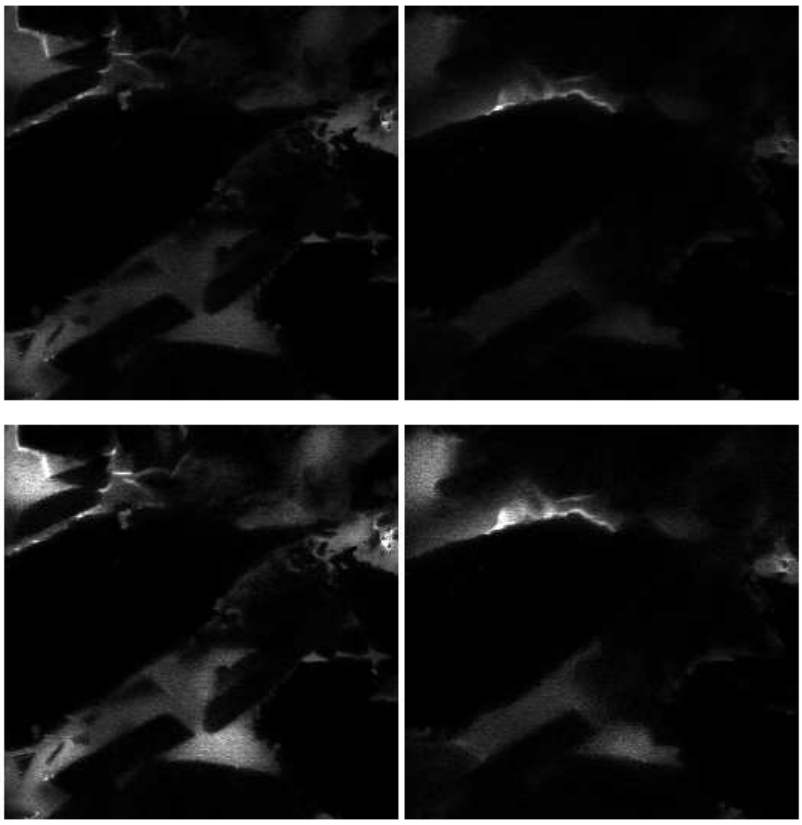

Figure 6. *Restoration of the sandstone CSLM image.*
First row: the attenuated CSLM images; second row: restoration by the FFT method. In each row, the fourth and seventh layer is displayed from left to right.

condensation' developed in [6] in order to reduce the computation time, still has a computational complexity of $\vee(N_z^2)$, as compared to $\vee(N_z \log N_z)$ for our method. Thus, when the number of vertical layers gets larger the difference in computational efficiency becomes increasingly pronounced. For spatially varying image densities the restoration quality using our method is a little poorer than in the layer method. This may be further improved by using a 'cumulant' estimator instead of the 'moment' estimator (3.6) [4].

The method of this paper was applied to a CSLM image of a geological sample consisting of sandstone cavities filled with a fluorescent oily substance, showing the practical usefulness of the method.

Acknowledgements The authors thank F.C.A. Groen and T.D. Visser for many useful discussions. T.D. Visser also kindly made the source code of the layer stripping algorithm and the CSLM data available to us.

Appendix

We perform some estimates for substantiating the numerical results of Section 4. The

CSLM transform can be written as

$$f(\mathbf{r}) = \rho(\mathbf{r}) \left(\int d\xi \; p_f(\xi) \exp\left(-\epsilon X(\xi)\right) \right) \times \left(\int d\xi \; p_b(\xi) \exp\left(-\epsilon X(\xi)\right) \right), \tag{A1}$$

where

$$p_f(\xi) = \frac{\sin\theta\cos\theta}{\pi \sin^2\omega}, \quad p_b(\xi) = \frac{\sin\theta}{2\pi(1-\cos\omega)}, \tag{A2}$$

with $\xi := (\theta, \phi)$. Here $X(\xi)$ is defined by

$$X(\xi) = \int_0^z \frac{dz'}{\cos\theta} \; g\left(\rho(\mathbf{r}')\right), \tag{A3}$$

where $\mathbf{r}' := \hat{r}(\mathbf{r}; \theta, \phi, z')$.

The total error $\mathcal{E}(\mathbf{r})$, being the difference between the exact density $\rho(\mathbf{r})$ and the approximation $\tilde{\rho}(\mathbf{r})$, can be estimated by a sum of two terms,

$$\mathcal{E}(\mathbf{r}) = |\rho(\mathbf{r}) - \tilde{\rho}(\mathbf{r})| \leq |\rho(\mathbf{r}) - f(\mathbf{r})| + |f(\mathbf{r}) - \tilde{\rho}(\mathbf{r})|, \tag{A4}$$

which we now consider separately.

For the first term, we have

$$|\rho(\mathbf{r}) - f(\mathbf{r})| = |\rho(\mathbf{r})| \left| 1 - \left(\int d\xi \; p_f(\xi) \exp\left(-\epsilon X(\xi)\right) \right) \times \left(\int d\xi \; p_b(\xi) \exp\left(-\epsilon X(\xi)\right) \right) \right| \tag{A5}$$

Now,

$$\begin{aligned} & 1 - \left(\int d\xi \; p_f(\xi) \exp\left(-\epsilon X(\xi)\right) \right) \times \left(\int d\xi \; p_b(\xi) \exp\left(-\epsilon X(\xi)\right) \right) \\ & = \int\int d\xi d\xi' p_f(\xi) p_b(\xi') \left\{ 1 - e^{-\epsilon(X(\xi)+X(\xi'))} \right\} \\ & \leq \int\int d\xi d\xi' p_f(\xi) p_b(\xi') \left\{ \epsilon(X(\xi) + X(\xi')) \right\} \end{aligned} \tag{A6}$$

where we have used the inequality $e^{-x} \geq 1 - x, \quad x \geq 0$. Denoting by $\rho_{\max}$ and $g_{\max}$ the maximum values of $\rho(\mathbf{r})$ and $g(\rho(\mathbf{r}))$ when $\mathbf{r}$ runs over the sample volume, we have

$$\left| \int d\xi \; p_i(\xi) X(\xi) \right| \leq \int d\xi \; p_i(\xi) \left| X(\xi) \right| \leq \int d\xi \; p_i(\xi) \frac{1}{\cos\omega} z g_{\max} = \frac{z g_{\max}}{\cos\omega}.$$

Substituting this in (A6) and the resulting formula in (A5) we get

$$|\rho(\mathbf{r}) - f(\mathbf{r})| \leq |\rho(\mathbf{r})| \frac{2\epsilon z g_{\max}}{\cos\omega} \leq \frac{2 g_{\max} \rho_{\max} \epsilon z}{\cos\omega}, \tag{A7}$$

where we have used that $f(\mathbf{r}) \leq \rho(\mathbf{r}) \leq \rho_{\max}$.

The second term to be estimated is

$$\begin{aligned} |\tilde{\rho}(\mathbf{r}) - f(\mathbf{r})| &= \epsilon \left| f(\mathbf{r}) \right| \times \left| \int d\xi \; \left(p_f(\xi) + p_b(\xi) \right) \int_0^z \frac{dz'}{\cos\theta} g\left(f(\mathbf{r}') \right) \right| \\ &\leq \; \epsilon \left| \rho(\mathbf{r}) \right| \times \int d\xi (p_f(\xi) + p_b(\xi)) \int_0^z \frac{dz'}{\cos\theta} g_{\max} \\ &\leq \; \frac{2 g_{\max} \rho_{\max} \epsilon z}{\cos\omega}. \end{aligned} \tag{A8}$$

Combining (A7) and (A8) we arrive at our final estimate for the total restoration error:

$$\mathcal{E}(\mathbf{r}) \leq \frac{4 g_{\max} \rho_{\max}}{\cos\omega} \epsilon z. \tag{A9}$$

This result confirms our previous observation (see Section 4) that the restoration error is roughly proportional to the product ϵz.

References

1. Abramowitz M. and I.A. Stegun (1972). *Handbook of Mathematical Functions*. Natl. Bur. Standards U.S.A., Washington.
2. Brakenhoff G.J., P. Blom and P. Barends (1979). Confocal scanning light microscopy with high aperture immersion lenses. *J. of Microscopy* 117, pp. 219-232.
3. Press W.H., B.P. Flannery, S.A. Teukolsky and W.T. Vetterling (1986). *Numerical Recipes, the Art of Scientific Computing*. Cambr. Univ. Press, New York.
4. Roerdink J.B.T.M. (1992). FFT-based methods for nonlinear image restoration in confocal microscopy. *Submitted*.
5. Van der Woude J.W. (1991). System identification of lossless layered media from input-output data. *Signal Processing* 22, pp. 269-285.
6. Visser T.D., F.C.A. Groen and G.J. Brakenhoff (1991). Absorption and scattering correction in fluorescence confocal microscopy. *J. Microscopy* 163, pp. 189-200.
7. Wilson T. and C.J.R. Sheppard (1984). *Theory and Practice of Scanning Optical Microscopy*. Acad. Press, New York.